Geomechanics for Energy and the Environment 47 (2026) 100850

Contents lists available at ScienceDirect

Geomechanics for Energy and the Environment

journal homepage: www.elsevier.com/locate/gete

# Modelling 3D subsoil temperature evolution by combining deterministic-probabilistic approaches based on geostatistical conditional simulation

Sara Kasmaeeyazdi, Francesco Tinti [*,a]

*Department of Civil, Chemical, Environmental and Material Engineering of University of Bologna, Via Terracini, Bologna 28 - 40131, Italy*

ARTICLE INFO

*Keywords:*
geostatistical conditional simulation
subsurface urban heat island
ground temperature
shallow geothermal energy

ABSTRACT

Modelling the underground temperature variability is a key element in geothermal energy designs which is affected by many parameters such as seasonal changing temperature of the surface, depth of bedrock, population density, etc. The most used approach is deterministic experimental models which can be modified and adapted based on a specific case study. Urban settlements dissipate heat in the ground, leading to uncertainties in defining temperature along depth. Regularly, the deterministic models of calculating subsoil temperature are valid for local areas and defined conditions, but fail to estimate the temperature evolution on the large-scale. In this research instead, the probabilistic approach - geostatistical multivariate conditional simulation - is tested to model the underground temperature variability using turning bands algorithm. A mixed urban-rural area (17 $km^2$), with availability of various log temperature measurements, as well as surface information on natural and anthropic factors, has been considered as the case study. Results highlighted the potential of using probabilistic models to recreate the 3D- temperature underground maps in space and time. In contrary of the deterministic models with a sharp discontinuity at bedrock, simulation results demonstrated the more consistent gradient change at the transitional zone between the sediments and the bedrock leading to improve the suitability maps quality and sustainable use of underground space specifically at large-scale levels. The main objective of this study is to test the proposed methodology. Due to the lack of available data under the specific conditions required for the analysis, synthetic boreholes were generated based on four real boreholes with temperature measurements. These synthetic datasets were then used as input for the methodology.

## 1. Introduction

Geothermal energy is a renewable energy source derived from the heat naturally stored in rocks and fluids deep within the earth's crust. It can help decarbonising heat consumption in homes, buildings and industry, then delivering emission reductions and at the same time increasing comfort for the households. Determination of the subsoil temperature is a crucial step for planning thermal energy projects for both heat, cool and power production. Hence, starting from available temperature measurements and hydrogeological information, it is possible to estimate temperature at different levels and consequently to provide a cost-effectiveness analysis of the sustainable exploitation of geothermal resource. Notable examples of modelling the subsurface urban heat island effect (SUHI) can be found in many cities, for example Milan, Italy[1,2] and Zurich.[3] Ngarambe et al. performed a comprehensive catalogue of SUHI research in various parts of the world.[4] Many authors have used the standard distance-weighted estimator to map temperature in 2-dimensional (2D) space at specific depths,[5,6]. However, to estimate the geothermal potential of a geological body at the required depth, it is fundamental to determine the temperature at any point in a 3-dimensional (3D) space. One of the main factors influencing the subsurface temperature distribution is the geothermal heat flow.[7] Moreover, in shallow layers (down to 50 m depth), other factors such as climate seasonality, ground thermal insulation, conditioned by geology and hydrogeology, and urban ground warming intervene as well.[8,9]

*Abbreviations:* 2D, two-dimensional; 3D, three-dimensional; BHE, borehole heat exchanger; GIS, geographic information system; GSHP, ground source heat pump; SUHI, subsurface urban heat island; TB, turning bands.

* Corresponding author.
*E-mail address:* francesco.tinti@unibo.it (F. Tinti).
[a] https://orcid.org/0000-0002-6750-9368

https://doi.org/10.1016/j.gete.2026.100850
Received 1 October 2025; Received in revised form 2 June 2026; Accepted 12 June 2026
Available online 13 June 2026

**Nomenclature**

| | |
|---|---|
| $a$ | variable term of the polynomial |
| $\alpha$ | thermal diffusivity ($m^2 \cdot s^{-1}$) |
| $A$ | temperature wave amplitude (K) |
| $b$ | constant term of the polynomial |
| $c$ | heat capacity ($J \cdot Kg^{-1} \cdot K^{-1}$) |
| $F$ | function |
| $g$ | Gaussian density function |
| $g^k$ | derivative of Gaussian density function |
| $\gamma$ | variogram |
| $h$ | distance among realizations (m) |
| $h_f$ | geothermal heat flow ($W \cdot m^{-2}$) |
| $H_k$ | Hermite Polynomial |
| $\lambda$ | thermal conductivity ($W \cdot m^{-1} \cdot K^{-1}$) |
| $\rho$ | density ($kg \cdot m^{-3}$) |
| $R$ | residual |
| $R_s^*$ | result of conditional simulation after back transform |
| $t$ | realization of the raw temperature variable (K) |
| $\tau$ | time (s) |
| $\tau_{T0}$ | time of minimum temperature (s) |
| $T$ | temperature (K) |
| $T_m$ | annual mean temperature (K) |
| $\nabla T_{geo}$ | geothermal gradient ($K \cdot m^{-1}$) |
| $T$ | wave period (s) |
| $x_1$ | length coordinate |
| $x_2$ | width coordinate |
| $x_3$ | height coordinate |
| $y$ | realization of the normalized temperature variable |
| $y_{cs}$ | conditional simulation |
| $y_{uc}$ | unconditional simulation |
| $y_{kc}$ | kriging estimation using the conditioned data |
| $y_{ku}$ | kriging estimation using the unconditioned data |

To record the past atmospheric temperature variations and recent global warming, the vertical temperature profiles (T-logs) can be measured in boreholes.[10–13] The measured values are influenced by the interaction between the deep ground temperature, the surface air temperature, and the heat transport in geological formations.[3]

The presence on the surface of paved areas and buildings modifies the natural ground temperature gradient. The man-induced thermal alterations, of different magnitude and period, can significantly change the ground temperature down to several tens of meters in the subsurface.[14,15] Moreover, recently researchers have started to correlate anthropogenic impact of buildings and structures to microbial evolution, thus evidencing the environmental issue of understanding the subsoil temperature in urban contexts.[16] SUHI can increase at least 50% of the energy stored in the subsurface. Bayer et al. have used analytical models to evaluate the influence of climate change and urban sources to ground temperature.[3] Four vertical measured temperature-depth-profiles had been considered in different urbanization areas, in the city and suburbs of Zurich. The result is coherent with the work on other central European cities, where large thermal anomalies in the upper urban ground, have been evidenced: Dublin,[17] Cologne,[18] Berlin.[19]

Recently, satellite derived data have also been used to determine the subsoil temperature, but the level of investigation is currently limited to very shallow depths.[20] Researchers have inserted, for the case study of the urban area of Beijing, land surface temperature values, remote sensing obtained, in a deterministic three-time-scale model to obtain subsurface temperature gradient. Calculation results were validated with measured soil temperatures at seven ground-based sites.

One common simplification of all these approaches is related to the deterministic modelling such as physical models account for urban heat sources increasing ground surface temperature. However, the deterministic heat transfer models applied are limited by unavoidable approximations, caused by local unpredictable influences.[21] Moreover, the scale affects the result, since enlarging the study area implies propagating the incertitude and its related error in the deterministic model. Uncertainty is due to the difficult quantification of ground layers properties and the impossibility to identify all the heat sinks and sources affecting the subsoil. The result is a high variability in space and time of the real values of ground temperature that is commonly neglected in 2D and 3D GIS supported models.

It has been understood that, due to the complexity of the problem and the variability of effects in an urban area, statistical, Machine Learning (ML) and geostatistical approaches are needed to improve the estimation of ground temperature models.[22] Recently, statistical approaches have been applied by several researchers, such as statistical clustering with regression decision tree,[23,24] spatial regression with Moran's I coefficient,[25] and Random Forest ML algorithm.[26] Kreitmar et al., at first, developed a statistical method able of grouping ground volumes into archetypes according to common thermal behaviours. They applied the methodology on the subsurface of the city of London as case study.[23] Afterwards, they expanded the approach, by also introducing the potential to exploit geothermal heat from the ground. The new methodology was applied on the subsurface of the cities of Cambridge, UK, and Berkeley, USA.[24] Chu and Rotta Loria used statistical and ML methods considering the relative locations of available information. In both works, the subsoil of Chicago was taken as case study.[25,26] On the other hand, geostatistical approaches provide quantitative descriptions of natural variables distributed in space or in time and space,[27] and can be used to predict ground temperature space and time variability in an urban area.[28]

Mostly, to understand the predominant conductive thermal regime, it is necessary to reproduce the temperature variation in 3D grid. To estimate the temperature at unsampled locations, some authors have used the Kriging interpolation method,[29] whose main advantages is considering the spatial variability in estimation process and the calculation of uncertainty associated with the predicted value.[30–32] As an example, Agemar et al. used Universal Kriging to accommodate a trend in data which is essential for the estimation of subsurface temperatures.[33] The same procedure was adopted by Kasmaee et al. for the estimation of temperatures in a mountain environment and inside a tunnel.[34] Moreover, the method has been used both for local subsurface temperature predictions[35] and for wide 3D temperature model.[36]

As a result of numerous and various factors affecting ground temperature, one estimation based on limited information could be just one image (the average) of all possible equiprobable alternatives. This issue affects temperature estimation results, where the available measurements are insufficient, in relation to the variability factors and the size of the domain. Since several outcomes can be produced by geostatistical simulation, reproducing the characteristics of the input variable and respecting the initial constrains can be considered as advantages. However, the results of a simulation should be analyzed due to the background of the application, to consider if the model is specified well, beyond its statistical parameters.[27] Geostatistical simulation is widely used to predict complex variables and to quantify uncertainty in a spatial context, in different fields such as mineral resources evaluation, reservoir characterization, hydrology, soil and environmental sciences.[37–39] Specifically to the geothermal sector, it is widely used for predicting the petrophysical properties of the hot fluids reservoirs, especially permeability, but it is not used to directly estimate the ground temperature variation.[40,41]

As the novelty, in this paper, geostatistical simulation techniques are used to characterize the ground temperature in the first 50 m below the ground surface, whose realizations are affected by ambient seasonal variations, subsurface urban heat island, groundwater movements and geothermal heat flow.

The conditional simulation technique has been applied on a case study, the urban area of Zurich city, for which extensive research on ground temperature had already been done and extended measurements at various locations were available.[3] The final result for the selected area is a set of prediction images of subsurface temperature, together with the distribution of equiprobable values. The aim of the present work is to set up a procedure to apply the geostatistical simulation for the definition of variability of ground temperature profiles in the urban context, starting from accessible, widespread and relatively cheap sets of measurements. The proposed scheme is based on combining deterministic and stochastic modelling of temperature evolution and it is supposed to gain the attention of policy makers and city planners.

## 2. Materials and methods

To obtain realistic pictures of spatial variability of one or more variables, conditional geostatistical simulation can be considered as an appropriate qualitative approach, especially for complex procedures such as numerical modelling of a dynamic system or economic optimization of a natural resource.[42] The aim is constructing realizations that reproduce the spatial variability of a regionalized variable/or values of the coregionalization in multi variate case, over a given domain. To perform the conditional simulation, a stochastic model should be used to describe the spatial distribution of the regionalized variable or coregionalized variables (object of the simulation), and an algorithm that constructs the realizations of this model (method of simulation).[27,43] The regionalized or coregionalized variable/s can be modeled by Gaussian random fields, using different types of algorithms[44] to coherently recreate the variable distribution and spatial correlation structure. Among available algorithms, Turning Bands (TB) is the one proposed by Matheron,[45] which can be performed in a multi-dimensional space simulation through a series of one-dimensional simulations. The advantages of the TB algorithm are the fast calculations and an accurate reproduction of the spatial correlation structure (in univariate and multivariate cases), even with distributions slightly different from the target ones.[46]

The TB algorithm generates 3D simulation results from several independent 1D simulations along lines that can be rotated in 3D space. In the multi-variable cases, to perform the simulation of coregionalized variables, there is a need of cross-covariance functions, which can model the relationships between the different variables. There are several approaches for modelling simple and cross-covariances[37] that can be used according to the spatial variability of available measured data (ex. the temperature measurements of boreholes). To construct realizations conditioned to a set of measured data, supplementary steps are required.

In the first step, the target area of interest should be identified for simulation of temperature spatial variability, conditioned by some limited measured temperature in vertical boreholes. It is common that temperature variability in subsurface area shows trend (continuous increase or decrease of temperature) in vertical direction.[47–49] Once defined an interest area of investigation, and the size, shape and dimension of the desired grid, the steps of the stochastic approach to simulate the ground temperature evolution are presented as follows:

Collection of all direct and indirect measurements of temperature in the study zone. Possibly the measurements should be regularly distributed all around the area of interest (See Paragraph ↱2.1);
Collection of geological, thermophysical, climate and geothermal information and use for the deterministic calculation of ground temperature profiles in all nodes of the grid; the 3D matrix of ground temperature (at a defined time) will be the collocated variable of the geostatistical simulation process (See Paragraph ↱2.2);
Removal of the ground temperature trend for both measured (step 1) and calculated (step 2) temperature values and calculation of residuals (See Paragraph ↱2.3);
Performing the steps of the geostatistical simulation: normal score transform of residuals, direct and cross variograms, conditional simulation of residuals by application of TB, back-transform of simulation results (See Paragraph ↱2.4);
Addition of trend to the back-transform results and final calculation of ground temperature (See Paragraph ↱2.5).

Collected data in steps 1 and 2 allow creating the ground temperature values, measured and calculated, for further comparison of direct and cross variograms of residuals, basis of the geostatistical simulation. The steps' details are presented below in paragraphs from ↱2.1 to ↱2.5, while Fig. 1 provides a schematic view of the workflow, showing how the collected data are inserted into the steps of the process, and how they interrelate each other to the final result, the set of equiprobable images of ground temperature.

### 2.1. Necessary measurement data

The initial data to be collected are the following:
Punctual measurements:

- Temperature profiles in boreholes, wells and pits;
- Climate data;
- Ambient temperature in the underground space (railway, underground lines, cellars, etc.);
- Surface temperature with contact probes and thermal infrared cameras;
- Lab and site tests on thermal diffusivity and conductivity of different soils and rocks;

Wide area information:

- Geological formations and depth of bedrock;
- Aquifers and surface water;
- Land use;
- Population density;
- Climate history;
- Aerial thermal images[50].

Some of these data provide direct information on actual temperature. They are inclusive of the subsurface urban heat island (SUHI) contribution and many other unpredictable heat sources in city context. The others provide indirect information over temperature. They can be inserted in the deterministic models to calculate hypothetical temperature profile values, which do not consider local variability and heterogeneity. Table 1 provides a list of the information/data, derived according to the use (direct/indirect) and specifying if they are punctual or distributed in the wide area.

### 2.2. Reconstruction of hypothetical standard behavior through deterministic analysis

The basic equation for defining the vertical distribution assessment of temperature ($T_g$) is a function of the ambient temperature wave, the thermal properties of the ground layers and the geothermal gradient.[8] Since all the variables entering the function are regionalized, the target variable is four dimensional, varying in space ($x_1$, $x_2$, $x_3$) and time ($t$). Having $T_g$ a sinusoidal behaviour, the year is usually chosen as a wave period. Eq. 1 summarizes the well-known distribution of temperatures in the subsoil.[51]

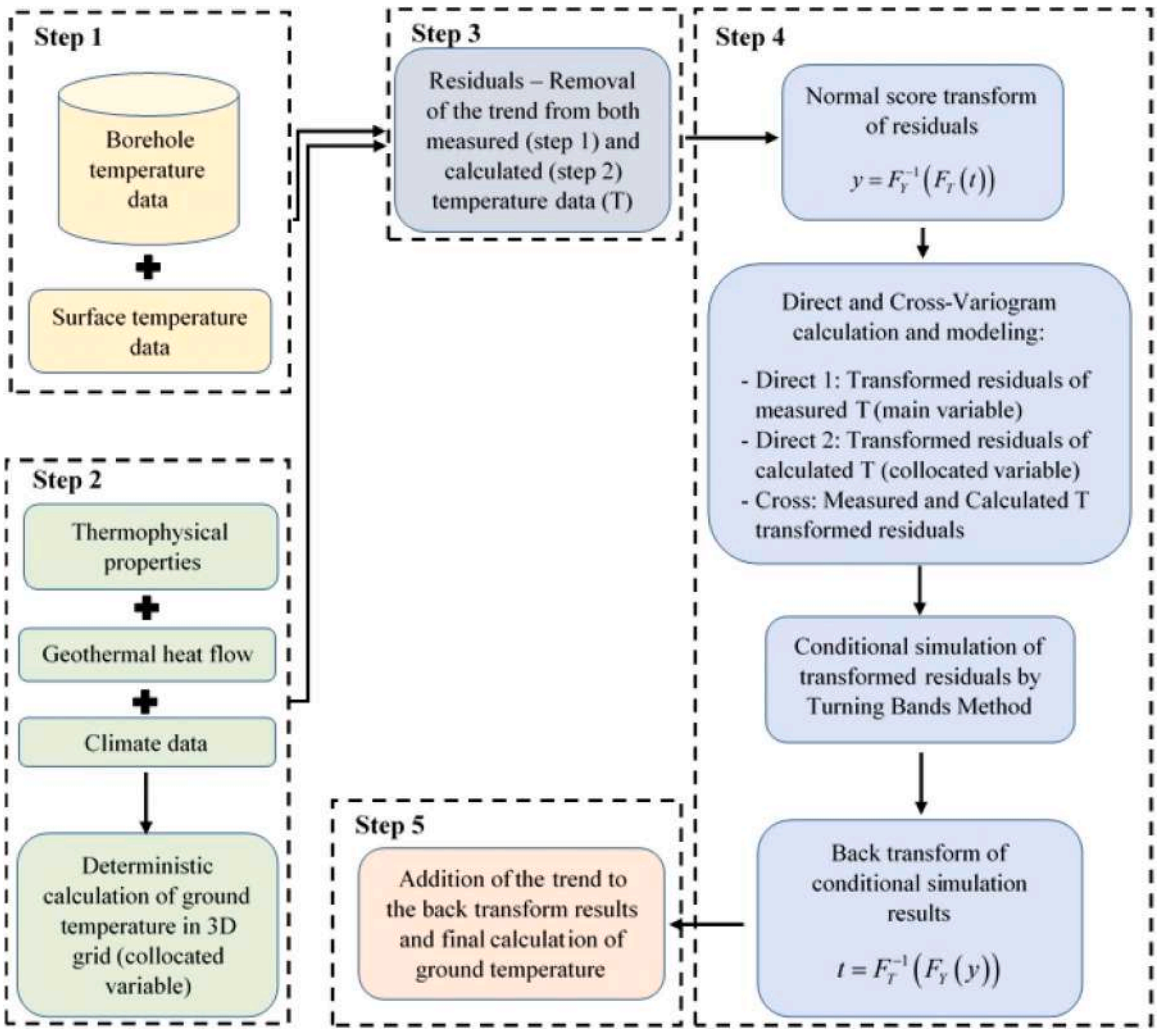


**Fig. 1.** Workflow of the methodology developed to simulate the ground temperature evolution in a stochastic environment.

**Table 1**
Information and data that can be acquired.

| | Direct measurements of temperature | Indirect information, to be inserted in the models |
|---|---|---|
| **Punctual measurements** | Temperature profiles in boreholes, wells and pits | Climate data |
| | Ambient temperature in the underground space (railway, underground lines, cellars, etc.) | Lab and site tests on thermal diffusivity and conductivity of different soils and rocks |
| | Surface temperature with contact probes and thermal infrared cameras | |
| **Wide area information** | Aerial thermal images | Geological layers |
| | | Aquifers and surface water |
| | | Land use |
| | | Population density |
| | | Climate history |

$$T(x_1,x_2,x_3,\tau) = T_m(x_1,x_2) - A(x_1,x_2)\cdot\exp\left[-x_3\cdot\sqrt{\left(\frac{\pi}{T\cdot\alpha(x_1,x_2,x_3)}\right)}\right] \cdot\cos\left[\frac{2\cdot\pi}{T}\cdot\left(\tau-\tau_{T_0}(x_1,x_2)-\frac{x_3}{2}\cdot\sqrt{\frac{T}{\pi\cdot\alpha(x_1,x_2,x_3)}}\right)\right] + \vec{\nabla}T_{geo}\cdot x_3 \quad (1)$$

Where $T_m$ is the annual surface average temperature at location $x_1x_2$ (°C), $A$ is the wave amplitude at location $x_1x_2$ (°C), the year is the wave period, $x_3$ is depth (m), $\tau$ is time (days), $\tau_{T0}$ is the time at minimum temperature (days), $\alpha$ is the equivalent thermal diffusivity on the depth of investigation (m$^2$/days) and $\vec{\nabla}T$ is the geothermal gradient at location $x_1x_2$ (°C/m), depending on geothermal heat flow $h_f$ (W/m$^2$) and equivalent thermal conductivity on the depth of investigation $\lambda$ (W/(m•K)) (see Eq. 2).

$$\vec{\nabla}T_{geo} = \frac{h_f(x_1,x_2)}{\lambda(x_1,x_2,x_3)} \quad (2)$$

When information on all the parameters is measured or estimated, it is possible to create a hypothetical 3D map of ground temperature $T$ in an interest area, by using the deterministic equation. An example of deterministic is presented by Tinti et al.[52] , who evaluated using temperature logs three 2D ground temperature profiles (far from buildings,

beside buildings and below buildings), in the countryside, varying for the different seasons. The analytical parameters selected for the present study (land use, population density, etc.) are varying based on the location of geothermal boreholes. However, these are information that can be obtained independently from boreholes' values and are available in various locations.

### 2.3. Removal of trend

Generally, ground temperature increases with depth due to the geothermal gradient. On the other hand, the gradient is affected by thermo-physical parameters of rocks crossed by the heat flow.[3,34,53] Many studies in different topics have shown the temperature trend in depth and near the ground surface influenced by the ground thermal conditions and the climate change.[3,34,47,54] In the mentioned case-studies, the temperature data are measured at different depths from boreholes, wells and in subsurface. Temperature varies with different slopes, depending on various parameters in a fixed time, and generally increasing with depth.[55] The presence of the trend poses an issue in applying geostatistical tools. When performing geostatistical estimation, a common solution is to keep such trend, by directly performing Universal Kriging. Instead, when performing geostatistical simulation, the temperature variable should be splitted in two parts (the trend $m$ and the residuals $R$, as simplified in Eq. 3). In this case, the simulation is performed directly on residuals (Eq. 4):[27]

$$T(x) = m(x) + R(x) \tag{3}$$

While:

$$m(x) = \sum_l a_l(x_0) \cdot f^l(x) \tag{4}$$

Where $m(x)$ is the trend, $f^l(x)$ are the given functions (usually monomials), $a_l$ are the unknown coefficients, and $R(x)$ is a zero mean stationary or intrinsic random residual.[27]

When the residuals subtract from the original data, which are assumed to be random, the mean of all $R(x)$ is zero. Conceptually, the spatial variability (represented by variograms and cross-variograms) can be performed on residuals and then simulation applied on residuals as well. In the case of vertical variability (ex. temperature variability in depth), Eq. 3 can be simplified as follows (Eq. 5):

$$T(x_1, x_2, x_3) = m(x_1, x_2, x_3) + b + R(x_1, x_2, x_3) \tag{5}$$

By fitting a polynomial function in the vertical direction, the residuals $R(x_1, x_2, x_3)$ can be obtained by subtraction.

### 2.4. Normal score transforms and conditional simulation

The idea of using conditional simulation consists in drawing different realizations of a variable meeting the experimental (measured) values at the data locations. The mentioned realizations are called conditional simulation to the experimental data. This conditioning deals with a certain robustness to the simulation with respect to the characteristics of the measured data.[56] The (conditional) simulation procedures rely on the (multi-) Gaussian framework and, therefore, require a prior transformation of the temperature variable ($T$) from raw to the Gaussian variable ($Y$),[43] whose realization is $y$ in Eq. 6.

$$y = F_Y^{-1}(F_T(t)) \tag{6}$$

Moreover, the back transformation of the Gaussian simulated results to the raw scale is necessary. The transformation fitted on data is called Gaussian anamorphosis. The most flexible approach for Gaussian anamorphosis is Hermite polynomials, which transfer a variable with a skewed distribution into a Gaussian one. The Hermite polynomials are defined as derivatives of the Gaussian density function as Eq. 7:[57]

$$H_k(y) = \frac{g^k(y)}{g(y)} = \frac{k^{th}\ derivative of\ Gaussian density}{Gaussian density} with k = 0, 1 \tag{7}$$

For a continuous variable like temperature, different simulation algorithms such as the TB, the spectral or the sequential methods can be used. The selected method depends on the spatial variability and the size of the area in question, the input data and the dimension of the output grid.[58] In multivariate applications, some of simulation algorithms may be challenging and require simplifications.[59,60] However, TB approach can obtain coherent realizations and generates 3D simulation results from several independent 1D simulations along lines that can be rotated in 3D space.[61] The conditional simulation $y_{cs}(x)$ of TB can be performed by two kriging parts and can be written as Eq. 8:

$$y_{cs}(x) = y_{uc}(x) + [y_{kc}(x) - y_{ku}(x)] \tag{8}$$

Where, $y_{uc}(x)$ is unconditional simulation value from TB, $y_{kc}(x)$ is kriging value using the conditioned data and $y_{ku}(x)$ is kriging value using the unconditioned simulated values.

### 2.5. Insertion of trend into back transform results

After performing the conditional simulation, reproduction of the spatial correlation structure can be obtained through different realizations of simulation. Since simulating the target variable $y(x)$ is performed on transformed data, the back transformation of the Gaussian simulated results to the raw scale is necessary:

$$t = F_T^{-1}(F_Y(y)) \tag{9}$$

Finally, by adding the residuals into the variable, the variability of the phenomena can be obtained:

$$T(x_1, x_2, x_3) = m(x_3) + b + R_S^*(x_1, x_2, x_3) \tag{10}$$

Where $R_s^*(x_1, x_2, x_3)$ is the result of conditional simulation after back transformation. The trend function is the same as the one used to remove the trend.

## 3. Case study

The effect of urban areas on the ground temperature gradient was studied using four ground temperature measurements in the Zurich city area, named Southeast, South, East and Central.[3] The Southeast borehole, 280 m deep, is located in the suburb of the Meilen old residential area. The South borehole, 200 m deep, is located on the western side of the Zurich Lake, in a recently built area with presence of industries. The East borehole, 400 m deep, is located at the Köllikerstrasse residential area, composed mainly by family houses with courtyards. Finally, the Central borehole, 400 m deep, is located in the Zurich city centre at the Rämistrasse, with the highest building density and few green spaces. Groundwater effects were found negligible in the whole area, since during drilling no water inflow was observed and no advective distortions of measured ground temperature could be perceived. Moreover, the four boreholes cross similar lithologies, mainly composed by sediments in the shallow layers. Consolidated fine sand of the Upper Freshwater Molasse (Tertiary) is the main lithological type, overlain by young Quaternary moraine deposits, of different thicknesses for the four boreholes. The thermophysical properties were considered for both surface moraine deposits and deeper consolidated fine sand layers. Initially, instead of assuming two distinguished values for the two geological layers, the same values were used; by using the developed deterministic algorithm including the bedrock depth,[28,36] the initial thermophysical values returned for the consolidated fine sand below a different ground temperature behaviour result from the shallow moraine deposits. In such way, it was possible to focus the study on the effect of bedrock depth on ground temperature evolution when crossing

**Table 2**
Information over the four boreholes.

| Borehole number | Location | Longitude | Latitude | X ED50 UTM28N | Y ED50 UTM28N | Moraine thickness (m) | Borehole depth (m) |
|---|---|---|---|---|---|---|---|
| 1 | South | 8.54390 | 47.31006 | 2274,000 | 5514,990 | 53 | 200 |
| 2 | Central | 8.55022 | 47.37086 | 2273,000 | 5521,990 | 15 | 540 |
| 3 | East | 8.56419 | 47.37442 | 2274,000 | 5522,990 | 26 | 200 |
| 4 | South-East | 8.65591 | 47.26705 | 2284,000 | 5513,990 | 0 | 280 |

geological discontinuities. This approach can be particularly helpful at the preliminary geothermal assessment stages, in absence of detailed information of thermophysical properties of the geological formations crossed.

Table 2 resumes the available information for the four boreholes.

Representative values for thermophysical properties of such sediments (both consolidated fine sand and moraine deposits) had been collected from the work of Bayer in 2016:[3]

- Thermal conductivity, $\lambda = 2.7$ W/(m·K);
- Bulk density, $\rho = 2700$ kg/m3;
- Heat capacity, $c = 700$ J/(kg·K);
- Thermal diffusivity, $\alpha = 1.43{\cdot}10\ {-}6$ m2/s.

The thermal properties found respect the relationship:

$$\alpha = \frac{\lambda}{\rho \cdot c} \tag{11}$$

Sensitivity analysis was previously conducted on the values of the four properties, and they have demonstrated that their variations within the admissible ranges would not seriously affect the quota of heat transfer underground. To correctly apply the geostatistical simulation method presented, the measurement data available for the interest area were not sufficient. Therefore, for the present preliminary work a synthetic case was created, starting from the available data. A set of credible temperature logs, 50 m deep, was recreated based on the mixed probabilistic-deterministic approach developed in the framework of the GEOTeCH European Project.[28]

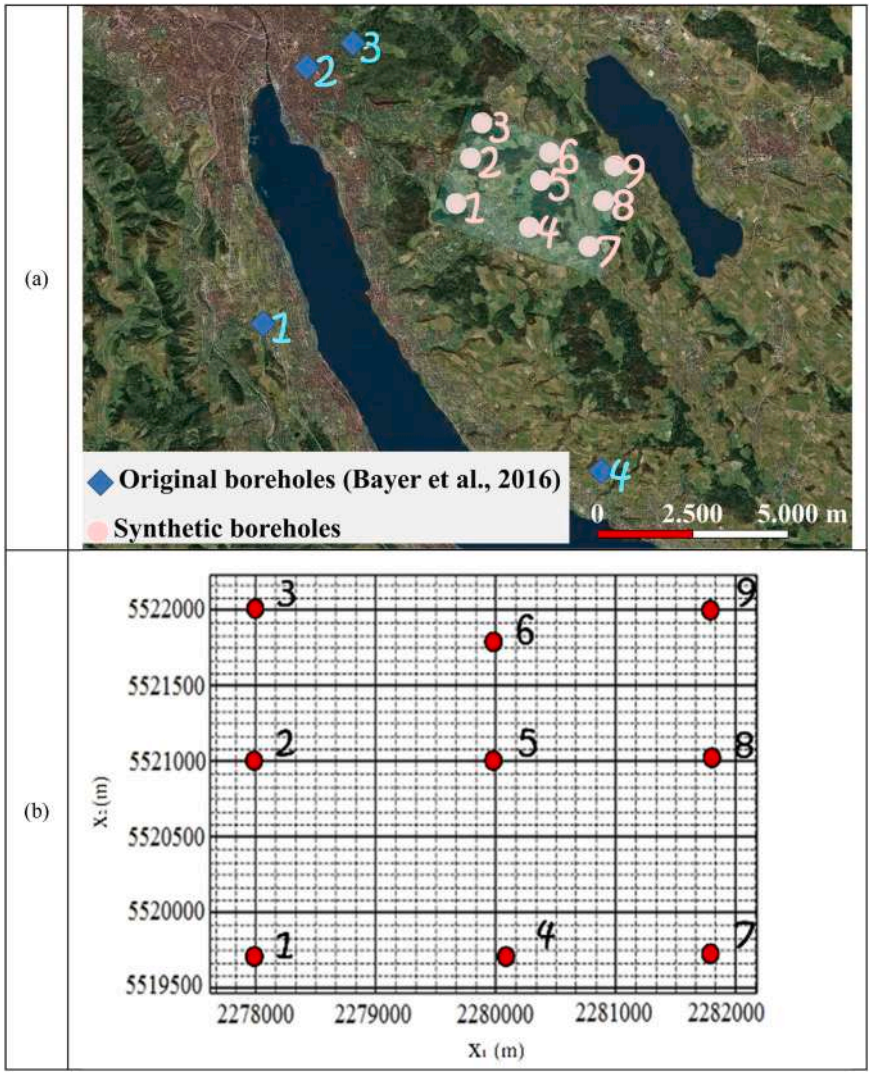


**Fig. 2.** Selected case study area, with evidence of the nine synthetic boreholes used for geostatistical simulation: over the satellite image (a); inside the regular grid (b).

The following steps were applied to create the nine synthetic boreholes:

- The available ground temperature measurements (Fig. 2**a**, boreholes 1, 2, 3 and 4) were used as input data.
- A grid with dimension 1 km x 1 km was created at the target area (Fig. 2**b**).
- Nine locations were selected as target points to create synthetic boreholes. The reasons behind the selection of the target area and the specific choice of the nine points are the following:

  No presence of water bodies and negligible groundwater effects;
  High variation of discontinuity between shallow moraine deposits and lower consolidated fine sand;
  High topographic variability, with presence of valleys and mountains;
  High population density variability, with presence of countryside, villages and rural areas.

- The geostatistical estimation technique of Universal Kriging was used to estimate the temperature values (also along depth) in the nine coordinates at the selected locations.

For the geostatistical simulation analysis, the main variable and the collocated variable had to be selected. The estimated ground temperature values in the nine boreholes (either in urban and rural area) were used as main variable for the following analysis. On the other hand, the basic deterministic calculation of ground temperature - not SUHI affected - for the entire grid nodes of the selected area was used as collocated variable.

Finally, a correlation analysis was performed between the ground temperature deviation in the measured area and the presence of urbanization (identified by global land cover and population density), in order to include SUHI in the final result.

By using the synthetic boreholes, the basic deterministic calculation of ground temperature - not SUHI affected - for the entire grid nodes of the selected area, is used as collocated variable to perform the geostatistical simulation. The area selected is in the suburbs of Zurich, comprising the villages of Zumikon (4711 inhabitants), Maur (9032 inhabitants) and Zollikerberg (12,791 inhabitants), for a total area of 16.66 km$^2$ (4.9 × 3.4 km$^2$). The altitude varies between 438 and 716 m a.s.l. The population density varies between 775 and 4316 inhabitants per square kilometre. The nine synthetic boreholes created using the described approach are almost equally spaced inside the area and they are shown in Fig. 2, with Coordinate Reference System ED50 / UTM28N

Boreholes n° 3, n° 5 and n° 9 fall in countryside, while n° 1, n° 2 and n° 8 are located beside the urban area and n° 4, n° 6 and n° 7 are inside the urban area.

For the selected area, the following maps have been built, by kriging interpolation of available information:

- Altitude map (Fig. 3-**left**, obtained based on EEA[62]);
- Bedrock depth map (Fig. 3-**right**, obtained based on Pelletier et al.[63]);
- Population map (Fig. 4-**left**, obtained based on CIESIN[64]);
- Surface temperature map, including the effect of buildings (Fig. 4-**right**, calculated based on the procedure described in Kasmaee and Tinti[28]).

The four selected properties (altitude, bedrock depth, population and surface temperature) were independent from synthetic data and therefore, it was possible to collect the related information on the target area without inserting uncertainties to the work.

Bedrock depth was a particularly important information, to identify the lower limit of moraine deposits, over consolidated sand, for each point of the grid. Table 3 shows the main information and the calculated moraine thickness from Fig. 3 for the nine synthetic boreholes. The collected bedrock depth data allowed to assign to each of the nine synthetic boreholes the thickness of the shallow moraine deposits and that of the consolidated fine sand, considering the depth of each of the nine boreholes equal to 50 m.

The surface temperature map integrates climate information, including altitude effect, with urban heat contribution. For the purposes of the present synthetic work, it substitutes the remote thermal images of wide area, usually performed for the identification of urban heat island. March was selected as reference month for the temperature map. It is also the main variable added to the nine borehole measurements for all the nodes of the grid, which conditions the further geostatistical simulation. The temperature profile for the nine boreholes, comprising SUHI, obtained by performing the regression with global land cover and population density described in Kasmaee and Tinti,[28] synthetically represents the long-time monitoring of ground temperature in the selected boreholes. It is the main variable of the further geostatistical simulation. The histogram of temperature data for the month of March and related basic statistics are presented in Fig. 5.

Finally, Eq. 1 was used to calculate, for each point of the 3D grid, the theoretical temperature value, varying in time and not SUHI affected. The calculation has considered the discontinuity between the shallower moraine sediments and the deeper consolidated sand (See Fig. 3). The theoretical ground temperature is the collocated variable of the geostatistical simulation. Again, the calculated temperature data of March were extrapolated for the simulation further steps. The temperature data obtained from the nine boreholes were considered as measured data for conditional simulation using TB method. Following the procedures explained, the trend was removed from data and residuals were calculated from Eq. 5 (Fig. 6**a**). Then the Hermit polynomials were used to transform data into Gaussian distribution (Fig. 6**b**).

The normalized residuals were used to simulate (by TB) the temperature behavior in vertical direction up to 50 m and on the 100 × 100 × 1 m$^3$ grid cell. Total dimension of the grid was 3400 × 4900 × 50 m$^3$. The constructed grid has been limited from the top with the topography down to the desired depth. Since the study is focused on vertical direction, the spatial variability analysis of the temperature is performed in vertical direction (Fig. 7). An important

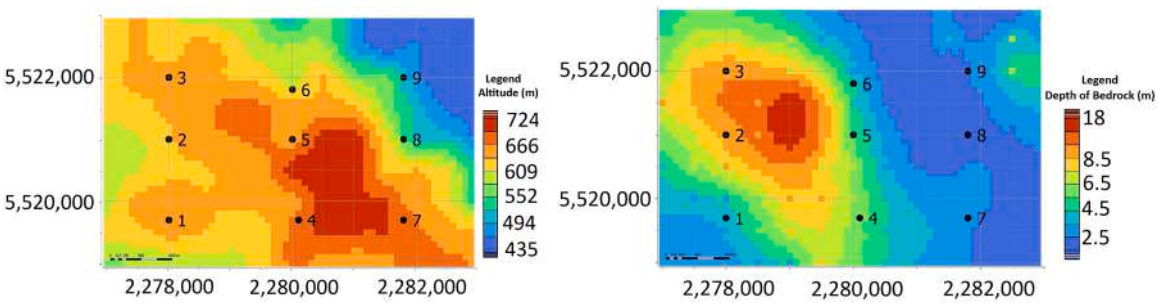


**Fig. 3.** Altitude (Left) and the Bedrock depth (Right) maps in the grid and borehole's locations.

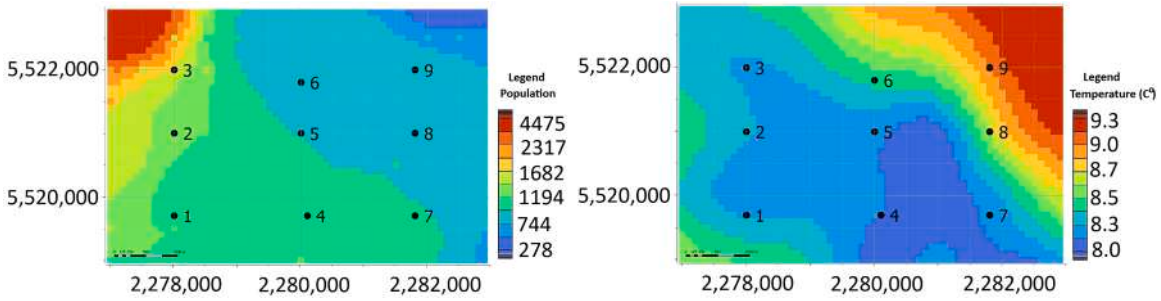


**Fig. 4.** Population (Left) and the Surface temperature (Right) maps in the grid and borehole's locations.

**Table 3**
Information over the nine synthetic boreholes.

| Synthetic borehole number | Longitude | Latitude | Thickness of moraine deposits (m) | Thickness of consolidated fine sand (m) |
|---|---|---|---|---|
| 1 | 8.60796 | 47.33857 | 3 | 47 |
| 2 | 8.61303 | 47.34929 | 8 | 42 |
| 3 | 8.61493 | 47.35753 | 10 | 40 |
| 4 | 8.63342 | 47.33300 | 5 | 45 |
| 5 | 8.63728 | 47.34400 | 4 | 46 |
| 6 | 8.64041 | 47.35057 | 4 | 46 |
| 7 | 8.65403 | 47.32849 | 3 | 47 |
| 8 | 8.65911 | 47.33920 | 2 | 48 |
| 9 | 8.66302 | 47.34744 | 2 | 48 |

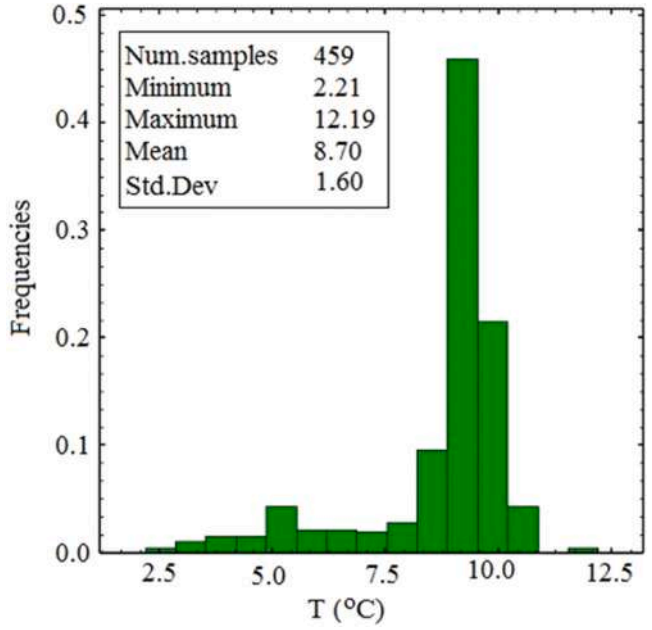


**Fig. 5.** Histogram and basic statistics of the ground temperature in the nine synthetic boreholes.

point to highlight is that TB simulation results are available for the whole grid, but the variogram analysis is performed only for vertical direction. The reason is that no consistent spatial structure was found in horizontal direction, but the horizontal variogram could be modelled as a pure nugget effect, with sill almost equal to the experimental variance (Fig. 8).

Therefore, for this case study, the main focus of the variogram analysis is on vertical direction and hence, all analysis is based on vertical variability.

Due to the complex physical quantitative behavior of subsoil temperature, the use of only nine boreholes' data cannot guarantee the validity of the simulated results of temperature in a large area. Therefore, there was a need to have an auxiliary variable as collocated variable (temperature data calculated from the deterministic function at all points of the grid). On the other hand, according to the authors experience,[49] to achieve the coherent results from experimental variograms, in order to fit the spatial variability of temperature, it was necessary to use more complex variogram models such as J-Bessel and K-Bessel,[27] specifically designed to represent the wave physical behavior of variables. The more complex variogram model is fundamental based on the many tests, authors performed to recreate the ground temperature behaviour, and the selected models were the best describing the physical behavior. Hence, the variogram model used for the conditional simulation was nested, composed by a nugget effect and three structures: 2 K-Bessel and 1 J-Bessel. The values of the model parameters are all different for the two direct variograms and for the cross variogram, and they are reported in Table 4.

The selected moving neighborhood for performing the simulation uses the searching distance of $500 \times 500 \times 20$ m with samples comprised between three and ten. The ellipsoid is divided in four sections, and minimum three samples from three sections are considered. The simulation and other geostatistical tools were undertaken using the ISATIS® software by Geovariances.[65]

## 4. Results and discussion

The conditional simulation was performed for 1000 realizations using TB algorithm. In order to confirm whether the realizations of a geostatistical simulation are worth representative of the reality – and so validating the simulation results – it is important to ensure that the simulated values have the same histogram as the experimental one of the available data of the main variable. That would mean that the histogram of simulated values is representative of the distribution of the main variable. Fig. 9 shows the Gaussian distribution of input data of the main variable and the histograms of simulation results for three different realizations, n° 500, 710 and 1000.

The results of the simulation, for all the 1000 realizations, behave very close to a normalized Gaussian distribution (mean = 0, standard deviation = 1). Besides, the data ranges have small deviations with respect to the main variable's initial data. Moreover, it is necessary to test the reproduction of the variogram model by the simulation results. It means comparing the experimental variograms of the realizations with the selected variogram model of the main variable. Fig. 10 shows the comparison between the experimental variograms of the realizations and the variogram model.

Fig. 10 has shown that, on average over the realizations, the variogram is well reproduced with the TB method, with a small deviation in the beginning that is influenced by the variogram model of the collocated variable. However, the simulation results converge with the variogram model of the main variable. Having proved that simulation results are coherent with the initial data, back transform was performed to get back the real variability of the phenomenon. The final value of

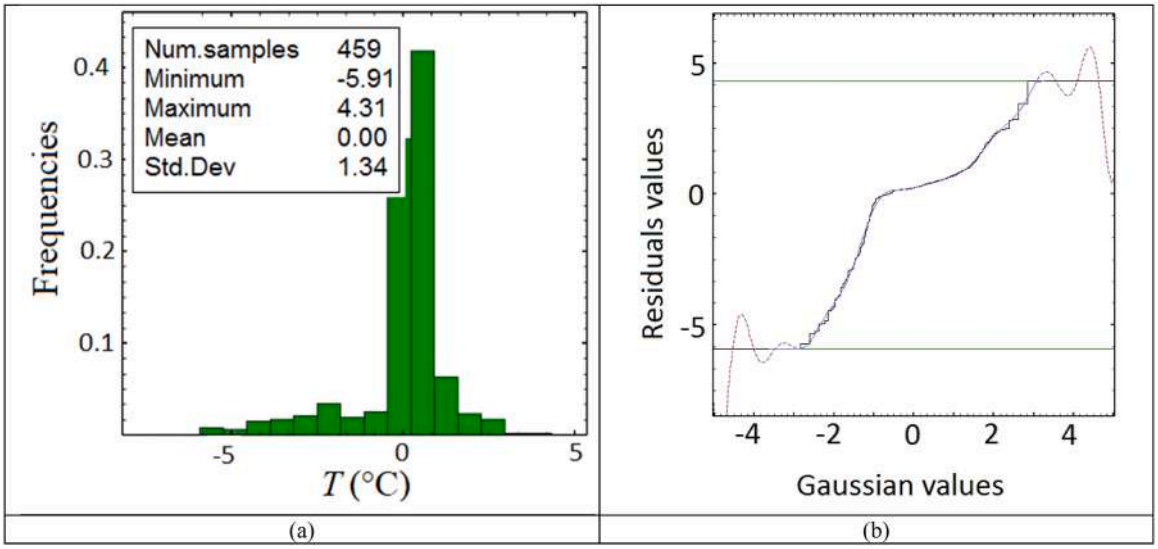


**Fig. 6.** Histogram of calculated residuals (a) and the anamorphosis function used for conversion between raw and gaussian space (b).

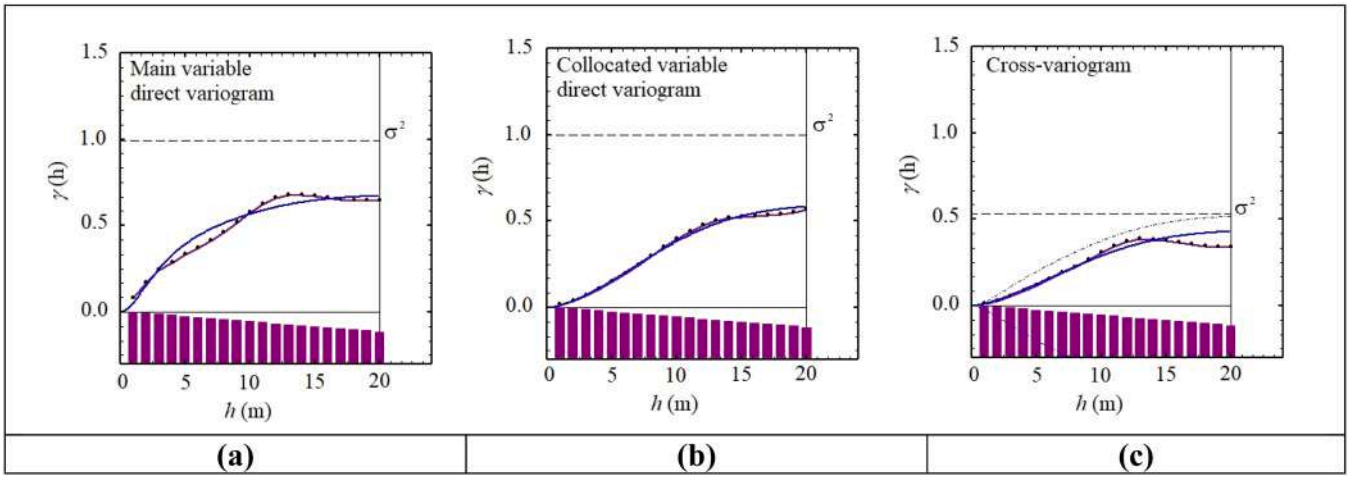


**Fig. 7.** Normalized direct and cross-sample vertical variograms (purple line and black points) with the fitted models (blue lines) used for the conditional simulation; purple bars: number of pairs.

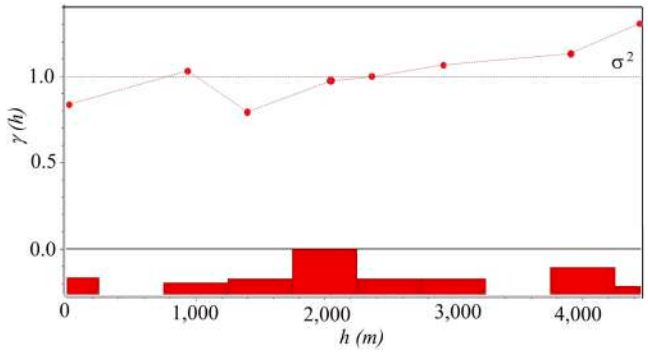


**Fig. 8.** Normalized horizontal experimental variogram of temperature (red dots) with the histogram of the numbers of pairs.

temperature prediction for the selected month of March was obtained by adding the removed trend to the residuals. Results are presented in Fig. 11 for three points (a, b, c) in vertical direction of the grid: point 220 (a), point 639 (b) and point 1284 (c). Point 220 was selected being the closest to an initial borehole log (specifically, borehole n°1) beside urban area. Point 639 was selected since it falls inside the urban area. Finally, point 1284 was selected since it falls in the countryside.

Fig. 11 shows for each point three ground temperature trends: the simulated one (red color), the one calculated with deterministic function, without inclusion of building heat effect, the collocated variable (blue color) and the one calculated with mixed deterministic/probabilistic approach,[24] based on regression coefficients (orange color). Transitional zone from sediment to bedrock is not a straight horizontal line but presents smooth variations in depth. For the proper comparison, the orange curves have been newly created for the three points.

The simulation results follow the deterministic curve and mixed probabilistic deterministic temperature curve. Some specificities appear. At the very shallow depth, the simulation results are well matched with the orange curve, evidencing the impact of urban areas in ground heat transfer. Then, in vertical direction, two discontinuities arise for the orange curve: the end of influencing SUHI and the presence of bedrock. From that point on, the orange curve sticks to the blue curve (calculated from the deterministic function) with a sharp deviation at the point of bedrock face. On the other hand, the red curve representing the simulation results has a smoother behavior without abrupt changes,

**Table 4**
Variogram models and parameters.

| Variogram models | Nugget effect | Structure 1 K-Bessel | | | Structure 2 J-Bessel | | | Structure 3 K-Bessel | | |
|---|---|---|---|---|---|---|---|---|---|---|
| | | Range (m) | Sill | α (scaling parameter) | Range (m) | Sill | α (oscillation frequency) | Range (m) | Sill | α (scaling parameter) |
| Direct variogram on the main variable | 0.03 | 1.45 | 0.400 | 1.7 | 3 | 0.1 | 40 | 0.84 | 0.28 | 38 |
| Direct variogram on the collocated variable | 0.00 | 1.45 | 0.047 | 1.7 | 3 | 0.4 | 40 | 0.84 | 0.55 | 38 |
| Cross-variogram | 0.00 | 1.45 | 0.050 | 1.7 | 3 | 0.25 | 40 | 0.84 | 0.39 | 38 |

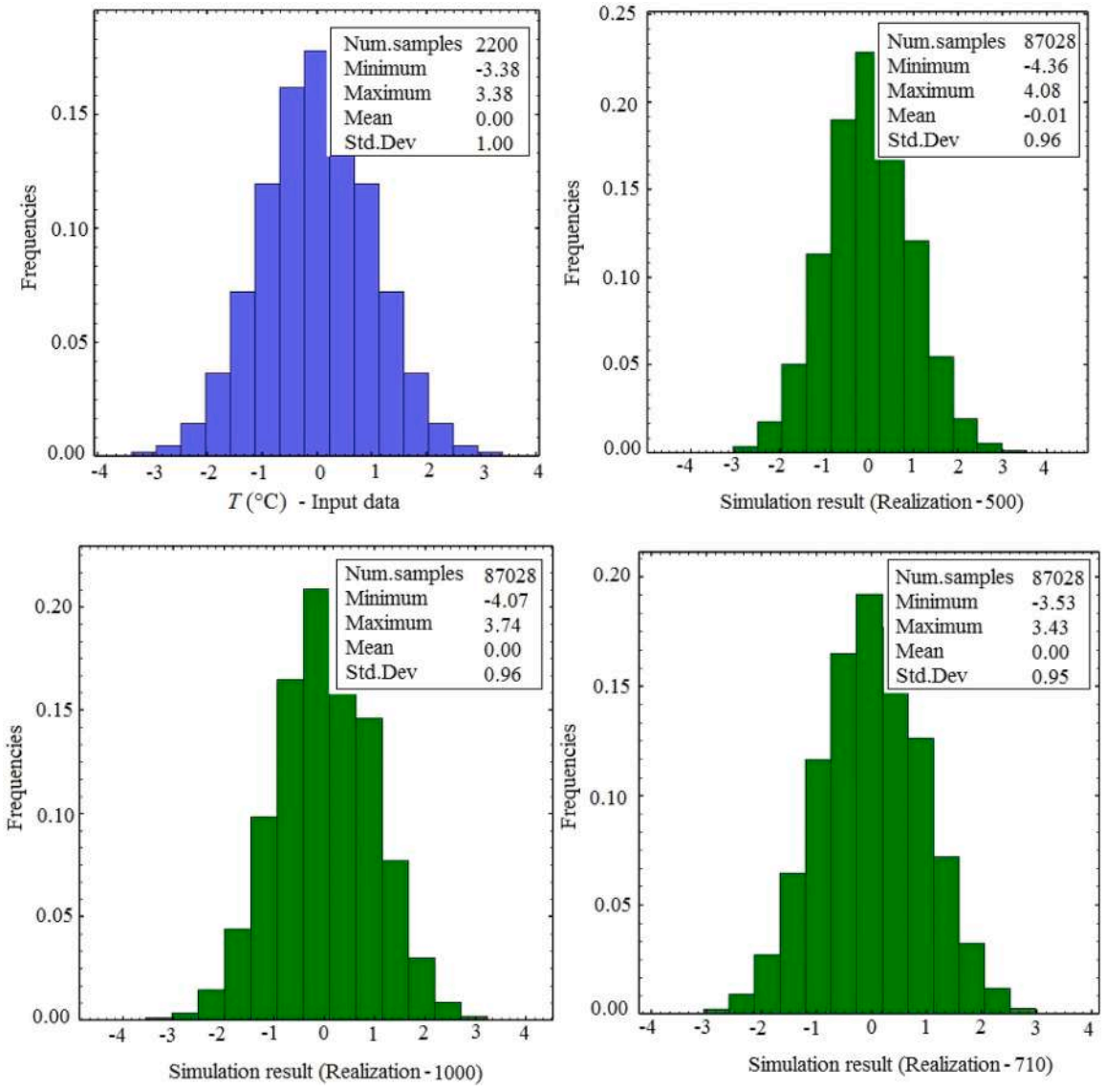


**Fig. 9.** Comparison between the histogram of the input data of the main variable (upper left, in blue) and the histograms of three realizations of the geostatistical simulation performed (green).

neither depending on the SUHI impact, nor on the thickness of sediments. By using the simple deterministic model, variations of the geothermal gradient depend exclusively on the variation of thermal conductivity, causing an abrupt change of ground temperature. However, the temperature variation along depth is much smoother and that can be obtained by integrating the simulation model results to the calculation. The geostatistical simulation results are affected by the number of data, both conditional and collocated. In this case study, the surface temperature data influenced by SUHI (main variable) and the deep stable ground temperature data (collocated variable) have important effect on the simulation results, especially on smoothing the temperature curve in the transition zone. In fact, the smoother behavior is more coherent to the transitional nature of the ground heat transfer and it should better approach the reality.[66,67] In Fig. 11, it can be seen that:

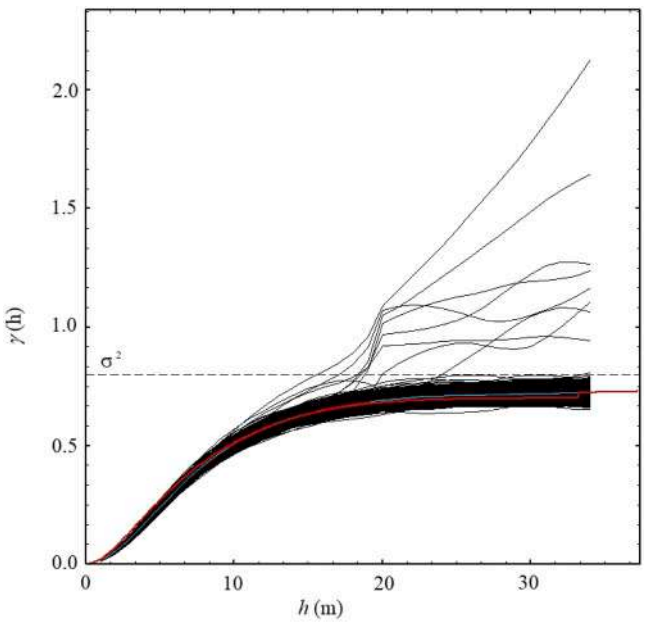


**Fig. 10.** Comparison among the variogram reproduction from 1000 realizations of geostatistical simulation (black lines), its average (cyan line) and the variogram model of the main variable (red line).

- Point a: This point, located beside urban area follows the deterministic behavior, but with a temperature shift of about 5°C with respect to the basic deterministic model. Maximum temperature reached is about 8°C at 5 m depth. The bedrock discontinuity zone is kept also in the simulation results;
- Point b: In this point, inside urban area, the simulated curve has higher temperature around 3.5–4°C than the deterministic calculated curve. The maximum temperature of 8°C is reached at 5 m. The bedrock discontinuity zone in both deterministic models show a large range of temperature variation (up to 6°C), while simulated curve smoothed into less than 1°C.
- Point c: it is located outside the urban area and is the one with the temperature curve closest to the standard one. The minimum temperature reached by the simulation results is about 3.5°C, which is 2°C more than the standard calculations.

Results of the probabilistic simulations in this work (Fig. 11) show that, in a large area, the temperature curve can be obtained using few measured data and considering the geological formations such as the presence of bedrock, even without detailed information on the building and land use. In contrast to the deterministic function that shows the sharp deviation of temperature curve facing the bedrock (Fig. 11-Blue line), the simulation results (Fig. 11-Red line) smooth the curve closer to the real behavior of the temperature gradient- obtained with temperature measurements in boreholes.[66,67] Researchers are currently ongoing to superimpose at small scale the land use and building effects to the natural ground heat flux. A recent notable example is the work of Rivera et al.[53] , who proposed an analytical solution for considering groundwater flow and land surface effects on thermal plumes of borehole heat exchangers (BHEs). The comparison of the analytical calculations on temperature measurements of an existing BHE placed in an urban area permitted them to state that the spatial and temporal changes in the top boundary temperature caused by different land use induce thermal anomalies on the ground that propagate in the subsurface, down to layers potentially occupied by the BHE. Therefore, the inclusion of land use variability is important for proper design of ground source heat pump (GSHP) systems. More recently, Focaccia et al.[68] have verified the thermal impact of a single building on the ground, by numerical simulation methods, including the specificities of the building itself, such as the presence of a cellar below a small portion of its volume. Spatial-temporal variability was considered by proper comparison with temperature logs below, beside and far from the studied building.

Both analytical and numerical solutions have proved to work efficiently at small scale, when details on land use, lithology and groundwater are known. Problems arise at large scale, with increasing variability (geological and hydrogeological), urban complexity and lack of proper information. Then, analysis has been conducted over the synthetic data extracted from limited boreholes in the site. The most consistent validation of results can be performed by planning targeted drillings considering various urban conditions as performed in this work to compare the real temperature variability. The method proposed in this paper, based on geostatistical simulation, can consider this variability, and could be integrated with both numerical and analytical design strategies. In real geothermal projects, both the main variable (ground temperature logs) and the collocated variable (analytical calculation of ground temperature) can be upgraded with respect to this synthetic work by adding information and performing more sophisticated calculations. Anyway, when dealing with large areas (a village, a district, or even a town), the complexity is too wide to be deterministically investigated node by node. Probabilistic simulation strategies should be therefore implemented, to get a realistic picture of the ground volume interested.

## 5. Conclusions

This study aimed at assessing the performance of probabilistic modelling (geostatistical conditional simulation using turning bands) to predict the temperature behavior along depth, conditioned by the presence of buildings. The methodology was performed over a case study, using synthetic data: main variable (conditioning data) and collocated variable. This choice was made, due to the limited number of boreholes with temperature logs in the specific condition required, as mentioned in Section 2. Despite this, the methodology and data validation procedures were performed in a comprehensive way, as a guideline for data analysis and methodology test, for further in-field research. By using the TB approach, it was possible to accurately reproduce the spatial correlation structure, measured by the direct and cross variograms of coregionalized variables under consideration. The deterministic function had evidenced a sharp discontinuity at the point of bedrock; however, the simulation results show the gradient change at the transitional zone between the sediments and the bedrock. Simulation studies need further steps, to consider the insertion of temporal variability inside the variogram modelling and to recreate the 4D map of temperature, varying in space and time. This should enhance the potential of ground heat transfer, by considering the high variability of ground temperature values, due to the multiple superposition of heat fluxes, especially present in-built environment, but impossible to deterministically precisely quantify at large-scale level. In fact, the application of geostatistical simulation for ground heat purposes can improve the quality of suitability maps for the use of ground source heat pumps and, more generally, for the sustainable use of underground space.

We propose the presented research as a basis for future geothermal potential assessment exploration campaigns, with temperature measurements aimed at testing the identified parameters on real datasets. The approach can subsequently be repeated and further validated by incorporating additional temperature logs and complementary indirect data to better constrain subsurface heat fluxes, as well as by extending the analysis to other, potentially larger, case study areas.

## CRediT authorship contribution statement

**Sara Kasmaeeyazdi:** Writing – review & editing, Writing – original draft, Visualization, Validation, Methodology, Investigation, Formal analysis, Data curation, Conceptualization. **Francesco Tinti:** Writing –

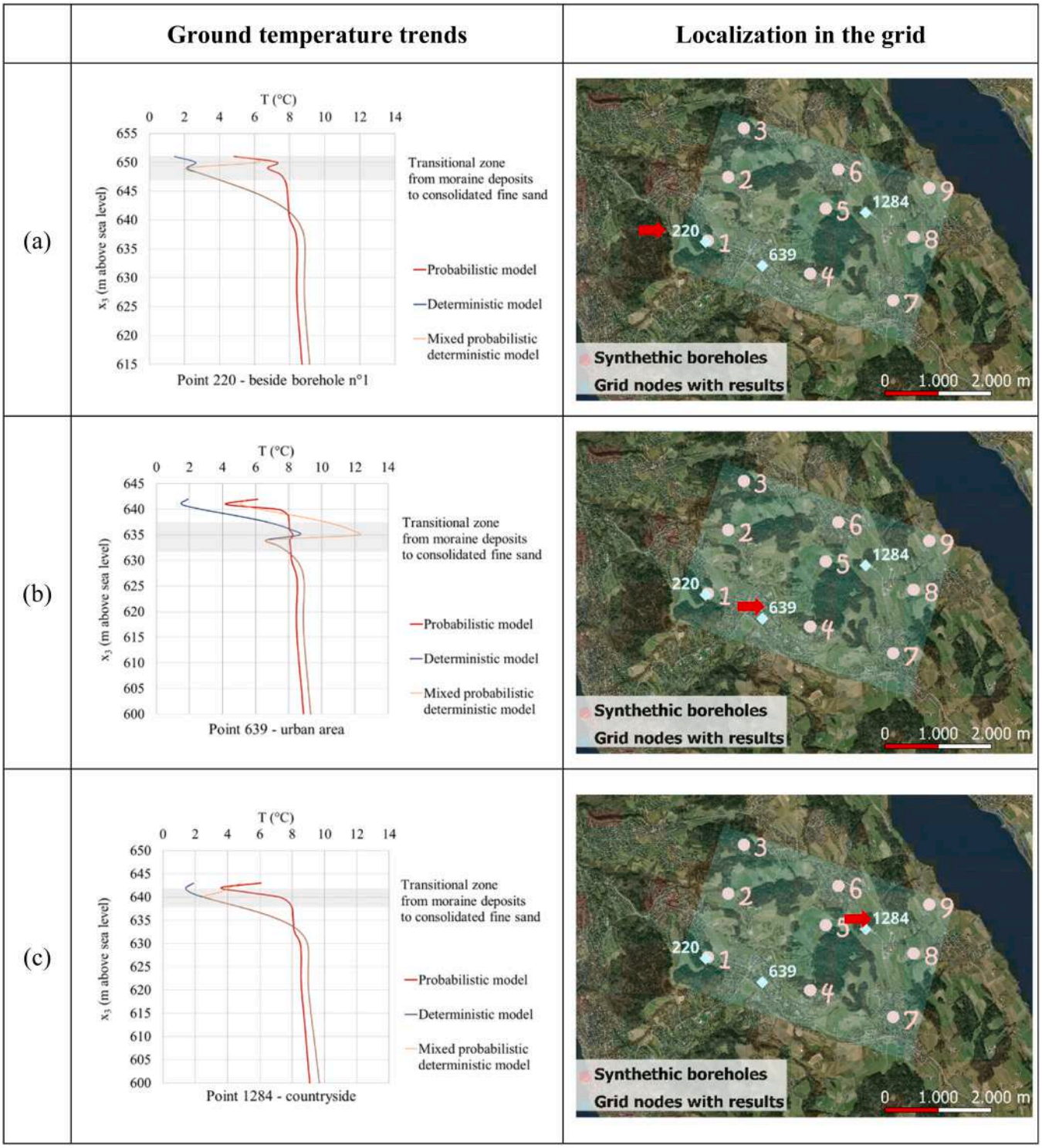


**Fig. 11.** Comparison of ground temperature behavior between the simulated results and the calculated data by simplistic deterministic functions, for three points of the grid: a (besides synthetic borehole 1), b (urban area) and c (countryside).

review & editing, Writing – original draft, Supervision, Data curation, Conceptualization.

## Declaration of Competing Interest

The authors declare that they have no known competing financial interests or personal relationships that could have appeared to influence the work reported in this paper.

## Data availability

Data will be made available on request.

## References

1. Previati A, Crosta G. Characterization of the subsurface urban island and its sources in the Milan city area, Italy. *Hydrogeol J*. 2021:2487–2500.

2. Previati A, Epting J, Crosta G. The subsurface urban heat island in Milan (Italy)- A modeling approach covering present and future effects on groundwater regimes (no) *Sci Total Environ*. 2022;810, 152119.
3. Bayer P, Rivera J, Schweizer D, Schärli U. Extracting past atmospheric warming and urban heating effects from borehole temperature profiles. *Geothermics*. 2016;64: 289–299.
4. Ngarambe J, Ray S, Yum GYoung. Subsurface urban heat islands: From prevalence and drivers to implications for geothermal energy and a proposed new framework based on machine learning (no) *Sustain Cities Soc*. 2025;120, 106153.
5. R. Schulz, R. Haenel and F. Kockel, *Geothermal Atlas of Europe - Federal Republic of Germany - West Federal States*, Gotha: Hurtig E., Cermak V., Haenel R., Zui V., 1992, pp. 34-37.
6. Hurter S, Schellschmidt R. Atlas of geothermal resources in Europe. *Geothermics*. 2003;32:779–787.
7. Cermak V, L. Rybach L. *Terrestrial heat flow in Europe, Verlag*. Springer; 1979.
8. Kusuda T, Achenbach P. Earth temperature and thermal diffusivity at selected stations in the United States. *ASHRAE Trans*. 1965;71:61–75.
9. Ferguson G, Woodbury A. Subsurface heat flow in an urban environment. *J Geophys Res*. 2004;109:2004.
10. Lachenbruch A, Marshall B. Changing climate: geothermal evidence from permafrost in the Alaskan Arctic. *Science*. 1986;234(4777):689–696.
11. Pollack H, Huang S. Climate reconstruction from subsurface temperatures. *Annu Rev Earth Planet Sci*. 2000;28:339–365.
12. Harris R, Chapman D. Mid-Latitude (30–60 N) climatic warming inferred by combining borehole temperatures with surface air temperatures. *Geophys Res Lett*. 2001;28(5):747–750.
13. Huang S, Pollack H, Shen P. A late Quaternary climate reconstruction based on borehole heat flux data, borehole temperature data, and the instrumental recoird (no) *Geophys Res Lett*. 2008;35:13703.
14. Claesson J, Hagentoft C. Heat loss to the ground from a building – I. General theory. *Build Environ*. 1991;12(4):173–179.
15. Hagentoft C, Claesson J. Heat loss to the ground from a building - II. Slab on the ground. *Build Environ*. 1991;26(4):395–403.
16. Noethen M, Becher J, Menberg K, et al. Environmental impact of an anthropogenic groundwater temperature hotspot. *Sci Total Environ*. 2024;955, 177153.
17. Allen A, Milenic D, Sikora P. Shallow gravel aquifers and the urban 'heat island' effect: a source of low enthalpy geothermal energy. *Geothermics*. 2002;32:569–578.
18. Zhu K, Blum P, Ferguson G, Baloke K, Bayer P. The geothermal potential of urban heat islands. *Environ Res Lett*. 2010;5(4):5.
19. Menberg K, Bayer P, Zosseder K, Rumohr S, Blum P. Subsurface urban heat islands in German cities. *Sci Total Environ*. 2013;442:123–133.
20. Zhan W, Ju W, Hai S, et al. Satellite Derived Subsurface Urban Heat Island. *Environ Sci & Technol*. 2014;48(20):12134–12140.
21. Kato S, Yamaguchi Y. Analysis of urban heat island effect using ASTER and ETM+ Data: separation of anthropogenic heat discharge and natural heat radiation from sensible heat flux. *Remote Sens Environ*. 2005;11(99):44–54.
22. Bayer P, Attard G, Blum P, Menberg K. The geothermal potential of cities. *Renew Sustain Energy Rev*. 2019;106:17–30.
23. M.J. Kreitmair, N. Makasis, A. Bidarmaghz, K. Menberg, R. Choudhary and K. Soga, "Finding common ground: A methodology for city-scale subsurface thermal modelling," *Urban Climate,* vol. 49, p. 101513, 49.
24. Makasis N, Kreitmair MJ, Chen K, Su Z, Choudhary R, Soga K. Finding common ground: A comparative study of city-scale shallow geothermal potential for Cambridge, UK, and Berkeley. *USA" Appl Energy*. 2026;403, 127062.
25. Chu Z, Rotta Loria AF. "Extending spatial regression to the analysis of subsurface urban heat islands,". *Urban Clim*. 2025;62, 102554.
26. Chu Z, Rotta Loria AF. "Modeling underground climate change across a city based on data about a building block,". *Sustain Cities Soc*. 2024;114, 105775.
27. Chiles J, Delfiner P. *Geostatistics Modeling Spatial Uncertainty*. 12th ed. WILEY; 2012.
28. Kasmaee S, Tinti F. A method to evaluate the impact of urbanization on ground temperature evolutiuon at a regional scale. *Rud Geol Naft Zb*. 2018;33(5):1–12.
29. G. Matheron, The Theory of Regionalized Variables And its Application, Paris: Centre de morphologie mathématique de Fontainebleau, Ecole Nationale Superieure des Mines, 1971.
30. M. Holdaway, "Spatial modeling and interpolation of monthly temperature using kriging," *Climate Research,* vol. 6, pp. 215-225.
31. Wu T, Li Y. Spatial interpolation of temperature in the United States using residual kriging. *Appl Geogr*. 2013;44:112–120.
32. Ruhaak W. "3-D interpolation of subsurface temperature data with measurement error using kriging. *Environ Earth Sci*. 2015;73:1893–1900.
33. Agemar T, Schellschmidt R, Schulz R. Subsurface temperature distribution in Germany. *Geothermics*. 2012;44:65–77.
34. Kasmaee S, Tinti F, Ferrari M, et al. Use of Universal Kriging as a tool to estimate mountain temperature distribution affected by underground infrastructures: the case of the Brenner Base Tunnel. *Eur Geotherm Congr Strasbg*. 2016.
35. Dose V, Menzel A. Bayesian correlation between temperature and blossom onset data. *Glob Change Biol*. 2006;12(8):1451–1459.
36. Tinti F, Kasmaee S, Elkarmoty M, Bonduà S, Bortolotti V. Suitability evaluation of specific shallow geothermal technologies using a GIS-based multi criteria decision analysis implementing the analytic hierarchic process. *Energies*. 2018;11(2):457.
37. Emery X. Statistical tests for validating geostatistical simulation algorithms. *Comput & Geosci*. 2008;34:1610–1620.
38. Boisvert J, Rossi M, Ehrig K, Deutsch C. Geometallurgical modeling at Olympic Dam Mine, South Australia. *Math Geosci*. 2013;45:901–925.
39. Rossi M, Deutsch C. *Mineral Resoirce Estimation*. 14. Dordrecht: Springer Science+ Business Media; 2014:332.
40. Ye Z, Wang GJ. Uncertainty analysis for heat extraction performance from a stimulated geothermal reservoir with the diminishing feature of permeability enhancement. *Geothermics*. 2022;100, 102339.
41. Vizi L, Fricvsky B, Zlocha M, Surovy M. Use of Geostatistical Simulation in Reservoir Thermodynamics Assessment and Interpretation at the Ďurkov Hydrogeothermal Structure, Slovakia. *Slovak Geol Mag*. 2020;20(1):85–98.
42. Dimitrakopoulos R. Conditional simulation algorithms for modelling orebody uncertainty in open pit optimization. *Int J Surf Min" Reclam Environ*. 2007;12(4): 173–179.
43. Lantuejoul C. *Geostatistical Simulation: Models and Algorithms*. Berlin: Springer; 2002.
44. Paravarzar S, Emery X, Madani N. Comparing sequential Gaussian and turning bands algorithms for cosimulating grades in multi-element deposits. *Compres Rendus Geosci*. 2015;347:84–93.
45. Matheron G. The intrinsic random functions and their applications. *Adv Appl Probab*. 1973;5(3):439–468.
46. Emery X, Lantuejoul C. TBSIM: a computer program for conditional simulation of three-dimensional Gaussian random fields via the turning bands method. *Comput Geosci*. 2006;32(10):1615–1628.
47. Békési E, Lenkey L, Limberger J, et al. Subsurface temperature model of the Hungarian part of the Pannonian Basin. *Glob Planet Change*. 2017.
48. Agemar T, Hese F, Moeck I, Stober I. List of criteria for the geothermal survey of deep-reaching faults in Germany. *Z der Dtsch Ges fur Geowiss*. 2017;168(2):285–300.
49. Tinti F, Boldini D, Ferrari M, et al. Exploitation of geothermal energy using tunnel lining technology in a mountain environment. A feasibility study for the Brenner Base Tunnel - BBT. *Tunn Undergr Space Technol*. 2017;70:182–203.
50. Mandanici E, Conte P, Girelli V. Integration of aerial thermal imagery, LiDAR data and ground surveys for surface temperature mapping in urban environments. *Remote Sens*. 2016;8(10):880.
51. Baggs S. Remote prediction of ground temperature in Australian soils and mapping its distribution. *Sol Energy*. 1983;30:351–366.
52. Tinti F, Barbaresi A, Ferrari M, et al. Experimental calibration of underground heat transfer models under a winery building in a rural area. *Rud Geol Naft Zb*. 2017;32 (3):15–22.
53. Rivera J, Blum P, Bayer P. Analytical simulation of groundwater flow and land surface effects on thermal plumes of borehole heat exchangers. *Appl Energy*. 2015; 146:421–433.
54. Dövényi P, Horváth F. A review of temperature, thermal conductivity, and heat flow data for the Pannonian BasinHorvath F, Royden LH, eds. *Pannon Basin" Am Assoc Petrol Geol Mem*. 1988;45:195–233.
55. Kubota Y, Suzuki N, Kimoto K, et al. Variation in subsurface water temperature and its kink to the Kuroshio Current in the Okinawa Trough during the last 38.5 kyr. *Quat Int*. 2017;452:1–11.
56. Journel A, Huijbregts C. *Mining Geostatistics*. Blackburn Press; 1978:600.
57. Wackernagel H. *Multivariate Geostatistics. An introduction with applications*. Berlin: Springer; 2003.
58. Beucher H, Renard D. *Reservoir characterization, Rapport technique du Centre de Géostatistique*. Ecole des Mines de Paris; 2005.
59. Almeida A, Journel A. Joint simulation of multiple variables with a Markov-type corregionalization model. *Math Geol" Math Geol*. 1994;26(5):565–588.
60. Gomez-Hernandez J, Journel A. Joint Sequential Simulation of Multi Gaussian Fields," in *Geostatistics Troia '92. Quantitative Geology and Geostatistics*. *Troia*. 1993.
61. Ren W. *Short note on conditioning turning bands realizations. Centr for Computational Geostatistics*. Edmonton: University of Alberta; 2005.
62. European Environmental Agency (EEA), 2004. Elevation map of Europe," [Online]. Available: ⟨https://www.eea.europa.eu/data-and-maps/data/digital-elevation-model-of-europe⟩.
63. Pelletier J, Broxton P, Hazenberg P, et al. A gridded global data set of soil, intact regolith and sedimentary deposit thickness for regional and global land surface modelling. *J Adv Model Earth Syst*. 2015;8:41–65.
64. CIESIN, Center for International Earth Science Information, "Documentation for the Gridded Population of the World, Version 4 (GPWv4)," Columbia Universit, Palisades NY, 2016.
65. Geovariances, *Isatis Software Manual,* Fontainableu, 2019.
66. Tang F, Nowamooz H. Long-term performance of a shallow borehole heat exchanger installed in a geothermal field of Alsace region. *Renew Energy*. 2018;128:210–222.
67. Tang F, Nowamooz H. Factors influencing the performance of shallow Borehole Heat Exchanger. *Energy Convers Manag*. 2019;181:571–583.
68. Focaccia S, Barbaresi A, Tinti F. Simulation of observed temperature field below a building in Bologna. *Environ Geotech*. 2017;7(4):295–305.